

Modeling the heterogeneous traffic flow considering the effect of self-stabilizing and autonomous vehicles

Yuan Gong(公元) and Wen-Xing Zhu(朱文兴)

Citation: Chin. Phys. B, 2022, 31 (**2**): 024502. DOI: 10.1088/1674-1056/ac2b18
Journal homepage: http://cpb.iphy.ac.cn; http://iopscience.iop.org/cpb

What follows is a list of articles you may be interested in

Three-dimensional clogging structures of granular spheres near hopper orifice

Jing Yang(杨敬), Dianjinfeng Gong(宫殿锦丰), Xiaoxue Wang(汪晓雪), Zhichao Wang(王志超), Jianqi Li(李建奇), Bingwen Hu(胡炳文), and Chengjie Xia(夏成杰)
Chin. Phys. B, 2022, 31 (**1**): 014501. DOI: 10.1088/1674-1056/ac2f2f

Modeling and analysis of car-following behavior considering backward-looking effect

Dongfang Ma(马东方), Yueyi Han(韩月一), Fengzhong Qu(瞿逢重), and Sheng Jin(金盛)
Chin. Phys. B, 2021, 30 (**3**): 034501. DOI: 10.1088/1674-1056/abc3b3

Game theory model of exit selection in pedestrian evacuation considering visual range and choice firmness

Wei-Li Wang(王维莉), Fang-Fang Wan(万芳芳), Siu-Ming Lo(卢兆明)
Chin. Phys. B, 2020, 29 (**8**): 084502. DOI: 10.1088/1674-1056/ab973a

A new car-following model with driver's anticipation effect of traffic interruption probability

Guang-Han Peng(彭光含)
Chin. Phys. B, 2020, 29 (**8**): 084501. DOI: 10.1088/1674-1056/ab9293

Traffic flow velocity disturbance characteristics and control strategy at the bottleneck of expressway

Jun-Wei Zeng(曾俊伟), Yong-Sheng Qian(钱勇生), Xu-Ting Wei(魏谞婷), Xiao Feng(冯骁)
Chin. Phys. B, 2018, 27 (**12**): 124502. DOI: 10.1088/1674-1056/27/12/124502

Modeling the heterogeneous traffic flow considering the effect of self-stabilizing and autonomous vehicles

Yuan Gong(公元) and Wen-Xing Zhu(朱文兴)†

School of Control Science and Engineering, Shandong University, Jinan 250061, *China*

(Received 16 August 2021; revised manuscript received 24 September 2021; accepted manuscript online 29 September 2021)

With the increasing maturity of automatic driving technology, the homogeneous traffic flow will gradually evolve into the heterogeneous traffic flow, which consists of human-driving and autonomous vehicles. To better study the characteristics of the heterogeneous traffic system, this paper proposes a new car-following model for autonomous vehicles and heterogeneous traffic flow, which considers the self-stabilizing effect of vehicles. Through linear and nonlinear methods, this paper deduces and analyzes the stability of such a car-following model with the self-stabilizing effect. Finally, the model is verified by numerical simulation. Numerical results show that the self-stabilizing effect can make the heterogeneous traffic flow more stable, and that increasing the self-stabilizing coefficient or historical time length can strengthen the stability of heterogeneous traffic flow and alleviate traffic congestion effectively. In addition, the heterogeneous traffic flow can also be stabilized with a higher proportion of autonomous vehicles.

Keywords: heterogeneous traffic flow, self-stabilizing effect, car-following model, autonomous vehicle

PACS: 45.70.Vn, 05.70.Fh, 05.70.Jk, 89.40.–a **DOI:** 10.1088/1674-1056/ac2b18

1. Introduction

Nowadays, the increasing number of cars has caused a series of problems such as traffic congestion and environmental pollution. The intelligent transportation system (ITS) aims to improve traffic efficiency, suppress traffic congestion, and reduce pollution. As a typical microscopic traffic flow model, the car-following model is widely used to investigate the driving behavior in the ITS environment. The classical car-following model was first proposed by Pipes[1] in 1953. In 1995, Bando *et al.*[2] improved Pipes' model and proposed the optimal velocity model (OVM). Nagatani[3] and Sawada[4] analyzed the traffic flow by nonlinear methods and found that the interaction of the next-nearest-neighbor can enhance the stability of traffic flow. Jiang *et al.*[5] constructed the full velocity difference model (FVDM), which considers both positive and negative velocity differences. Later, many scholars improved the traditional car-following model by incorporating different factors.[6–29] Ge *et al.*[6] extended the optimal velocity model by combining the effect of backward looking with the ITS environment. Li *et al.*[13,14] introduced the self-stabilizing control into the OVM and proved that traffic stability can be significantly strengthened via self-stabilizing control. Chen *et al.*[19] improved the car-following model by considering the expected effect and self-stabilizing effect. Peng[25] studied the relationship between traffic interruption probability and traffic flow stability based on an extended optimal velocity model.

In recent years, with the fast development of intelligence and automation, autonomous vehicles have attracted many researchers' attention.[30–34] Homogeneous traffic flow will gradually evolve into heterogeneous traffic flow in the next few years. To enable autonomous vehicles to drive cooperatively with human-driving vehicles, many scholars have carried out certain studies on the characteristics of the heterogeneous traffic system.[35–49] Zhu *et al.*[37] proposed a car-following model with adjustable sensitivity and smoothing factor, and used it to investigate the mixed traffic flow. Xie *et al.*[40] modeled heterogeneous traffic through a general car-following model framework, and demonstrated that connected vehicles play an important role in improving traffic efficiency. An *et al.*[42] put forward a car-following model with the discrete following interval for autonomous vehicles, and discussed the impact of discrete car-following interval on stabilizing mixed traffic flow. Wang *et al.*[43] researched the mixed traffic system from the aspects of controllability theory and optimal controller design. These studies analyzed the properties of heterogeneous traffic flow from different perspectives. However, most existing studies did not fully consider the effect of self-stabilizing in heterogeneous traffic flow. Therefore, this paper incorporates the self-stabilizing effect into the car-following model for heterogeneous traffic flow and proposes an improved car-following model, which enables the vehicle to use the information of both its own and other vehicles to jointly control its driving behavior.

The paper is organized as follows. Section 2 proposes a new car-following model for heterogeneous traffic flow. Section 3 gives the linear stability condition of the proposed model by linear stability analysis. Section 4 gives the mKdV equation and the kink-antikink solution of the model by nonlinear analysis. Section 5 conducts numerical simulations to verify the theoretical results. Finally, Section 6 concludes this paper.

†Corresponding author. E-mail: zhuwenxing@sdu.edu.cn

© 2022 Chinese Physical Society and IOP Publishing Ltd

2. Models

Figure 1 shows a heterogeneous traffic system mixed with human-driving and autonomous vehicles (human-driving vehicles are green and autonomous vehicles are orange). In this system, N vehicles distribute on a single-lane road without overtaking.

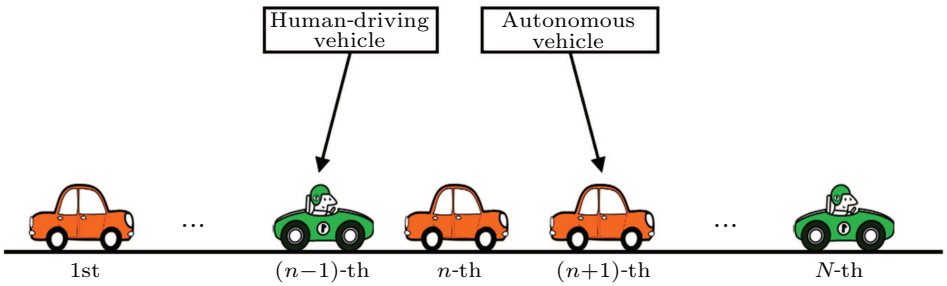


Fig. 1. The illustration of the heterogeneous traffic system with N vehicles.

2.1. Model for human-driving vehicles

The dynamic model for human-driving vehicles is constructed based on Bando's optimal velocity model (OVM)[2]

$$\frac{\mathrm{d}v_n(t)}{\mathrm{d}t} = \alpha_{\mathrm{H}}\left[V\left(\Delta x_n(t)\right) - v_n(t)\right], \tag{1}$$

where $\alpha_{\mathrm{H}} = 1/\tau_{\mathrm{H}}$ is the driver's sensitivity coefficient, τ_{H} is the driver's reaction time; $v_n(t)$ is the velocity of vehicle n at time t; $\Delta x_n(t) = x_{n+1}(t) - x_n(t)$ is the headway between vehicle n and vehicle $n+1$ at time t; $V\left(\Delta x_n(t)\right)$ is the optimal velocity function (OVF).

Based on the OVM, Li *et al.*[13] proposed an extended car-following model with the self-stabilizing effect, which considers the velocity of the vehicle at a historical time. It is formulated as

$$\frac{\mathrm{d}v_n(t)}{\mathrm{d}t} = \alpha_{\mathrm{H}}\left[V\left(\Delta x_n(t)\right) - v_n(t)\right] + \lambda\left[v_n(t) - v_n(t-t_0)\right], \tag{2}$$

where $v_n(t-t_0)$ is the velocity of vehicle n at the historical time $t-t_0$; $v_n(t) - v_n(t-t_0)$ is the self-stabilizing term, which means the difference between the current velocity $v_n(t)$ and the historical velocity $v_n(t-t_0)$; λ is the control coefficient.

Furtherly, Chen *et al.*[50] considered the continuous change of vehicle velocity in a historical time period, and presented a modified car-following model:

$$\begin{aligned}\frac{\mathrm{d}v_n(t)}{\mathrm{d}t} &= \alpha_{\mathrm{H}}\left[V\left(\Delta x_n(t)\right) - v_n(t)\right] \\ &\quad + \lambda\left[v_n(t) - \frac{1}{t_0}\int_{t-t_0}^{t} v_n(u)\,\mathrm{d}u\right],\end{aligned} \tag{3}$$

where t_0 is the historical time length; $\frac{1}{t_0}\int_{t-t_0}^{t} v_n(u)\,\mathrm{d}u$ denotes the average velocity of vehicle n at time $[t-t_0, t]$, which can describe the continuous velocity change of the vehicle in a historical time period; $v_n(t) - \frac{1}{t_0}\int_{t-t_0}^{t} v_n(u)\,\mathrm{d}u$ can be regarded as an extended self-stabilizing term, which represents the difference between the velocity of vehicle n at time t and its average velocity at time $[t-t_0, t]$; λ is the self-stabilizing coefficient.

In Chen's model,[50] the velocity of a vehicle in a historical period is taken into account in the effect of self-stabilizing, so the vehicle information can be utilized more sufficiently. Therefore, this paper uses Chen's model[50] as the car-following model for human-driving vehicles. The optimal velocity function is given as[51]

$$\begin{aligned}V\left(\Delta x_n(t)\right) &= \frac{v_{\max}}{2}\left[\tanh\left(0.13\left(\Delta x_n(t) - l_n\right) - 1.57\right)\right. \\ &\quad \left. + \tanh\left(0.13 l_n + 1.57\right)\right],\end{aligned} \tag{4}$$

where $v_{\max}$ represents the maximum velocity and l_n denotes the length of vehicle n. Furthermore, due to the heterogeneity of different drivers in real traffic, the sensitivity α_{H} can take different values for different drivers.

2.2. Model for autonomous vehicles

Autonomous vehicles can obtain information from other vehicles through sensors, such as the position and velocity of the front and back vehicles. Recently, Zhu *et al.*[37] proposed a new car-following model for autonomous vehicles by incorporating the backward headway into the OVM:

$$\frac{\mathrm{d}v_n(t)}{\mathrm{d}t} = \alpha_{\mathrm{A}}\left[V_{\mathrm{op}}\left(\Delta x_n(t), \Delta x_{n-1}(t)\right) - v_n(t)\right], \tag{5}$$

where α_{A} represents the sensitivity of the autonomous vehicle, and $V_{\mathrm{op}}\left(\Delta x_n(t), \Delta x_{n-1}(t)\right)$ is the generalized optimal velocity function:

$$\begin{aligned}&V_{\mathrm{op}}\left(\Delta x_n(t), \Delta x_{n-1}(t)\right) \\ &= (1+\mu)V\left(\Delta x_n(t)\right) - \mu V\left(\Delta x_{n-1}(t)\right),\end{aligned} \tag{6}$$

where $\mu \in (0, 0.5)$ is the smooth factor, and the expression of $V\left(\Delta x_n(t)\right)$ is the same as that in Eq. (4).

Similar to the model for human-driving vehicles (3), the autonomous vehicle can also use the position or velocity of the vehicle itself in the historical time period to realize self-stabilizing control. Then the autonomous vehicle can use the information of the current vehicle itself and other vehicles simultaneously during its driving process. Therefore, to better describe the driving behavior of autonomous vehicles, a new

car-following model with the self-stabilizing effect is established as follows:

$$\frac{\mathrm{d}v_n(t)}{\mathrm{d}t} = \alpha_{\mathrm{A}}\left[(1+\mu)V(\Delta x_n(t)) - \mu V(\Delta x_{n-1}(t)) - v_n(t)\right] + \lambda\left[v_n(t) - \frac{1}{t_0}\int_{t-t_0}^{t} v_n(u)\,\mathrm{d}u\right]. \tag{7}$$

Here, we assume that the self-stabilizing effect of autonomous vehicles has the same form as that of human-driving vehicles. The meaning of the parameters in Eq. (7) is the same as that in Eqs. (3) and (5). When $\lambda = 0$, the proposed model (7) reduces to model (5), which represents the model without self-stabilizing effect; when $t_0 \to 0$, from $\lim_{t_0\to 0}\frac{1}{t_0}\int_{t-t_0}^{t} v_n(u)\,\mathrm{d}u = v_n(t)$ we can obtain that model (7) also reduces to model (5).

2.3. A generic model for heterogeneous traffic flow

By comparing the equations of models (3) and (7), the two models can be rewritten into a unified form

$$\frac{\mathrm{d}v_n(t)}{\mathrm{d}t} = \alpha\left[(1+p)V(\Delta x_n(t)) - pV(\Delta x_{n-1}(t)) - v_n(t)\right] + \lambda\left[v_n(t) - \frac{1}{t_0}\int_{t-t_0}^{t} v_n(u)\,\mathrm{d}u\right]. \tag{8}$$

In this equation, α is the sensitivity of the vehicle, and the sensitivity of autonomous vehicles α_{A} is higher than that of human-driving vehicles α_{H}; p is the interaction coefficient between the current vehicle and the back vehicle. For autonomous vehicles, the interaction coefficient p is the smooth factor μ (see Subsection 2.2); for human-driving vehicles, the backward headway is not considered during driving, so p is equal to zero. Therefore, the interaction coefficient p is taken as

$$p = \begin{cases} \mu, & \text{for autonomous vehicles,} \\ 0, & \text{for human-driving vehicles,} \end{cases} \tag{9}$$

where $0 < \mu < 0.5$.

3. Linear stability analysis

In this section, the linear stability analysis of the proposed model is conducted. First, according to the mean value theorem of integrals, there exists $t_{\mathrm{m}} \in [0, t_0]$ such that $\frac{1}{t_0}\int_{t-t_0}^{t} v_n(u)\,\mathrm{d}u = v_n(t - t_{\mathrm{m}})$. Then the proposed model (8) is reformulated as follows:

$$\frac{\mathrm{d}v_n(t)}{\mathrm{d}t} = \alpha\left[(1+p)V(\Delta x_n(t)) - pV(\Delta x_{n-1}(t)) - v_n(t)\right] + \lambda\left[v_n(t) - v_n(t-t_{\mathrm{m}})\right]. \tag{10}$$

Furtherly, we can derive the following formula by performing the first-order Taylor expansion on $v_n(t - t_{\mathrm{m}})$:

$$v_n(t - t_{\mathrm{m}}) = v_n(t) - t_{\mathrm{m}}\frac{\mathrm{d}v_n(t)}{\mathrm{d}t}. \tag{11}$$

If equation (11) is substituted into Eq. (10), the following equation can be deduced:

$$\frac{\mathrm{d}v_n(t)}{\mathrm{d}t} = \frac{\alpha}{1-\lambda t_{\mathrm{m}}}\left[(1+p)V(\Delta x_n(t)) - pV(\Delta x_{n-1}(t)) - v_n(t)\right]. \tag{12}$$

Let $\alpha_{\mathrm{m}} = \alpha/(1-\lambda t_{\mathrm{m}})$, and then equation (12) can be rewritten into the following form:

$$F(\Delta x_n, \Delta x_{n-1}, v_n) = \frac{\mathrm{d}v_n(t)}{\mathrm{d}t} = \alpha_{\mathrm{m}}\left[(1+p)V(\Delta x_n(t)) - pV(\Delta x_{n-1}(t)) - v_n(t)\right], \tag{13}$$

where $F(\Delta x_n, \Delta x_{n-1}, v_n)$ is the acceleration function.

When the traffic flow reaches a steady-state equilibrium, the headway and velocity of vehicles are given by $\Delta x_n(t) = \Delta x_n^{\mathrm{eq}}$, $\Delta x_{n-1}(t) = \Delta x_{n-1}^{\mathrm{eq}}$, and $v_n(t) = v_n^{\mathrm{eq}}$. Then the traffic flow in a steady state must satisfy the following equation:

$$F\left(\Delta x_n^{\mathrm{eq}}, \Delta x_{n-1}^{\mathrm{eq}}, v_n^{\mathrm{eq}}\right) = 0. \tag{14}$$

Add a small disturbance to the steady-state solution: $\Delta x_n(t) = \Delta x_n^{\mathrm{eq}} + \delta\Delta x_n(t)$, $\Delta x_{n-1}(t) = \Delta x_{n-1}^{\mathrm{eq}} + \delta\Delta x_{n-1}(t)$, and $v_n(t) = v_n^{\mathrm{eq}} + \delta v_n(t)$. Inserting them into Eq. (13) and conducting the first-order Taylor expansion, we can derive the following linearized equation:

$$\frac{\mathrm{d}\delta v_n(t)}{\mathrm{d}t} = \underbrace{F\left(\Delta x_n^{\mathrm{eq}}, \Delta x_{n-1}^{\mathrm{eq}}, v_n^{\mathrm{eq}}\right)}_{=0} + F_n^{\Delta x}\delta\Delta x_n(t) + F_{n-1}^{\Delta x}\delta\Delta x_{n-1}(t) + F_n^{v}\delta v_n(t), \tag{15}$$

where

$$F_n^{\Delta x} = \left.\frac{\partial F}{\partial \Delta x_n}\right|_{\left(\Delta x_n^{\mathrm{eq}}, \Delta x_{n-1}^{\mathrm{eq}}, v_n^{\mathrm{eq}}\right)} = \alpha_{\mathrm{m}}(1+p)V'\left(\Delta x_n^{\mathrm{eq}}\right),$$
$$F_{n-1}^{\Delta x} = \left.\frac{\partial F}{\partial \Delta x_{n-1}}\right|_{\left(\Delta x_n^{\mathrm{eq}}, \Delta x_{n-1}^{\mathrm{eq}}, v_n^{\mathrm{eq}}\right)} = -\alpha_{\mathrm{m}} pV'\left(\Delta x_{n-1}^{\mathrm{eq}}\right),$$
$$F_n^{v} = \left.\frac{\partial F}{\partial v_n}\right|_{\left(\Delta x_n^{\mathrm{eq}}, \Delta x_{n-1}^{\mathrm{eq}}, v_n^{\mathrm{eq}}\right)} = -\alpha_{\mathrm{m}}.$$

Suppose that $\delta\Delta x_n(t) = \Delta X_n \exp(\mathrm{i}\omega n + st)$, $\delta\Delta x_{n-1}(t) = \Delta X_{n-1}\exp\{\mathrm{i}\omega(n-1) + st\}$, and $\delta v_n(t) = V_n \exp(\mathrm{i}\omega n + st)$, where ΔX_n, ΔX_{n-1}, and V_n are constants. According to $\Delta x_n(t) = x_{n+1}(t) - x_n(t)$ and $\frac{\mathrm{d}\Delta x_n(t)}{\mathrm{d}t} = v_{n+1}(t) - v_n(t)$, we can get

$$\Delta X_n = \frac{V_{n+1}\mathrm{e}^{\mathrm{i}\omega} - V_n}{s}, \tag{16}$$

$$\Delta X_{n-1} = \frac{V_n\mathrm{e}^{\mathrm{i}\omega} - V_{n-1}}{s}. \tag{17}$$

Incorporating Eqs. (16) and (17) into Eq. (15), we can obtain the following equation:

$$s^2 V_n = \alpha_{\mathrm{m}}\left[(1+p)V'\left(\Delta x_n^{\mathrm{eq}}\right)\left(V_{n+1}\mathrm{e}^{\mathrm{i}\omega} - V_n\right) - pV'\left(\Delta x_{n-1}^{\mathrm{eq}}\right)\left(V_n - V_{n-1}\mathrm{e}^{-\mathrm{i}\omega}\right)\right] - \alpha_{\mathrm{m}} s V_n. \tag{18}$$

Now let us consider the case of uniform traffic flow, where all vehicles have the same steady-state velocity and the same equilibrium headway. Then $V_n = V_{n+1} = V_{n-1}$ and $\Delta x_n^{\rm eq} = \Delta x_{n-1}^{\rm eq}$. Let $\Delta x_n^{\rm eq} = \Delta x_{n-1}^{\rm eq} = \Delta x^{\rm eq}$, and then we can reduce Eq. (18) to a simplified form

$$\begin{aligned} &s^2 + \alpha_{\rm m} s - \alpha_{\rm m} V'(\Delta x^{\rm eq}) \\ &\times[(1+p)\left(\mathrm{e}^{\mathrm{i}\omega} - 1\right) - p\left(1 - \mathrm{e}^{-\mathrm{i}\omega}\right)] = 0. \end{aligned} \tag{19}$$

Assume that the solution of Eq. (19) has the following form: $s = s_1(\mathrm{i}\omega) + s_2(\mathrm{i}\omega)^2 + \cdots$. After substituting it into Eq. (19) and ignoring the higher-order terms, we can solve the first- and second-order terms of $\mathrm{i}\omega$:

$$\begin{cases} s_1 = V'(\Delta x^{\rm eq}), \\ s_2 = \dfrac{(1+2p)V'(\Delta x^{\rm eq})}{2} - \dfrac{[V'(\Delta x^{\rm eq})]^2}{\alpha_{\rm m}}. \end{cases} \tag{20}$$

The necessary condition for a stable uniform traffic flow is $\mathrm{Re}(s) < 0$, *i.e.*,

$$\frac{(1+2p)V'(\Delta x^{\rm eq})}{2} - \frac{[V'(\Delta x^{\rm eq})]^2}{\alpha_{\rm m}} > 0. \tag{21}$$

By solving the above inequality and considering $\alpha_{\rm m} = \alpha/(1-\lambda t_{\rm m})$, the linear stability condition of the uniform traffic flow is derived as follows:

$$\alpha > \frac{2V'(\Delta x^{\rm eq})(1-\lambda t_{\rm m})}{1+2p}, \tag{22}$$

where the prerequisite $\lambda t_{\rm m} < 1$ must be satisfied.

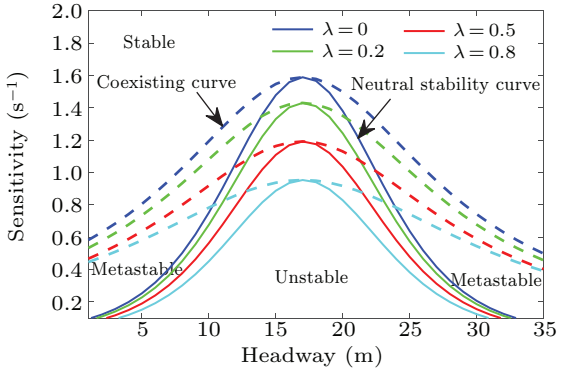


Fig. 2. Phase diagram in the headway-sensitivity space under different λ values.

According to the linear stability condition (22), we check the effect of different model parameters on the stability of traffic flow. The phase diagrams in the headway-sensitivity space under different parameters λ and $t_{\rm m}$ are plotted in Figs. 2 and 3, respectively. The solid lines represent the neutral stability curves, while the dashed lines denote the coexisting curves. As shown in Figs. 2 and 3, the phase diagram of the traffic flow can be divided into three different areas. Above the coexisting curve is the stable area, below the neutral stability curve is the unstable area, and between the two curves is the metastable area. Figure 2 shows that the self-stabilizing effect in the proposed car-following model can reduce the area of the unstable region, thereby making the traffic flow more stable. In addition, figures 2 and 3 suggest that the unstable area becomes smaller with the increase of the parameter λ or $t_{\rm m}$. From these figures, we can draw a conclusion that increasing the value of the parameter λ or $t_{\rm m}$ can enhance the stability of the traffic flow and suppress traffic congestion.

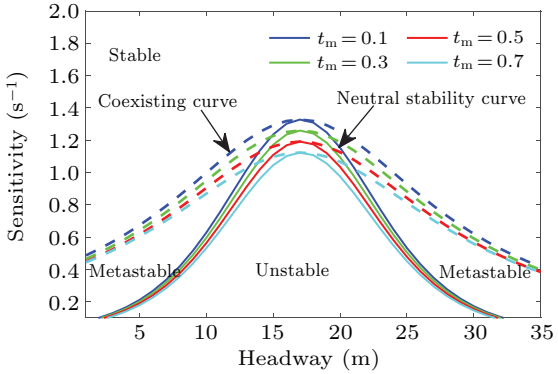


Fig. 3. Phase diagram in the headway-sensitivity space under different $t_{\rm m}$ values.

4. Nonlinear analysis

In this section, the nonlinear analysis is conducted to derive the mKdV equation of the proposed model. First, rewrite the model equation (10) to the following form:

$$\begin{aligned} \frac{\mathrm{d}^2\Delta x_n(t)}{\mathrm{d}t^2} = \alpha\Big\{ &(1+p)\left[V(\Delta x_{n+1}(t)) - V(\Delta x_n(t))\right] \\ &- p\left[V(\Delta x_n(t)) - V(\Delta x_{n-1}(t))\right] - \frac{\mathrm{d}\Delta x_n(t)}{\mathrm{d}t}\Big\} \\ &+ \lambda\left[\frac{\mathrm{d}\Delta x_n(t)}{\mathrm{d}t} - \frac{\mathrm{d}\Delta x_n(t-t_{\rm m})}{\mathrm{d}t}\right]. \end{aligned} \tag{23}$$

Considering the slow-changing behavior of long waves around the critical point $(h_{\rm c}, \alpha_{\rm c})$, we define slow variables X and T as follows:

$$X = \varepsilon(n + ht), \quad T = \varepsilon^3 t, \tag{24}$$

where n is the space variable, t is the time variable, and h is a constant. The headway can be set as

$$\Delta x_n(t) = h_{\rm c} + \varepsilon R(X, T). \tag{25}$$

Substituting Eqs. (24) and (25) into the model equation (23) and expanding the equation to term ε^5 yield the following nonlinear partial differential equation:

$$\begin{aligned} &\varepsilon^2 k_1 \partial_X R + \varepsilon^3 k_2 \partial_X^2 R + \varepsilon^4\left(\partial_T R + k_3 \partial_X^3 R - k_4 \partial_X R^3\right) \\ &+\varepsilon^5\left(k_5 \partial_X \partial_T R + k_6 \partial_X^4 R - k_7 \partial_X^2 R^3\right) = 0. \end{aligned} \tag{26}$$

The coefficients k_i are shown in Table 1, where $V' = \left.\frac{\mathrm{d}V(\Delta x)}{\mathrm{d}\Delta x}\right|_{\Delta x = h_{\rm c}}$ and $V''' = \left.\frac{\mathrm{d}^3 V(\Delta x)}{\mathrm{d}\Delta x^3}\right|_{\Delta x = h_{\rm c}}$.

Table 1. The coefficients k_i of the model.

k_1	k_2	k_3	k_4	k_5	k_6	k_7
$h-V'$	$h^2\tau(1-\lambda t_{\rm m})-[(1+2p)/2]V'$	$(\lambda\tau h^3 t_{\rm m}^2/2)-(V'/6)$	$V'''/6$	$2h\tau(1-\lambda t_{\rm m})$	$-[(1+2p)/24]V'-(\lambda\tau h^4 t_{\rm m}^3/6)$	$[(1+2p)/12]V'''$

If we take $h=V'$, then we can eliminate the second- and third-order terms of ε. Near the critical point $\tau_{\rm c}$, let

$$\frac{\tau}{\tau_{\rm c}}=1+\varepsilon^2, \tag{27}$$

where

$$\tau_{\rm c}=\frac{1}{\alpha_{\rm c}}=\frac{1+2p}{2(1-\lambda t_{\rm m})V'}.$$

Then equation (26) can be rewritten as follows:

$$\begin{aligned}&\varepsilon^4\left(\partial_T R-g_1\partial_X^3 R+g_2\partial_X R^3\right)\\&+\varepsilon^5\left(g_3\partial_X^2 R+g_4\partial_X^4 R+g_5\partial_X^2 R^3\right)=0.\end{aligned} \tag{28}$$

The coefficients g_i are shown in Table 2.

Table 2. The coefficients g_i of the model.

g_1	g_2	g_3	g_4	g_5
$(V'/6)-(\lambda\tau_{\rm c}h^3t_{\rm m}^2/2)$	$-V'''/6$	$h^2\tau_{\rm c}(1-\lambda t_{\rm m})$	$2h\tau_{\rm c}(1-\lambda t_{\rm m})\left((V'/6)-(\lambda\tau_{\rm c}h^3t_{\rm m}^2/2)\right)-[(1+2p)/24]V'-(\lambda\tau_{\rm c}h^4t_{\rm m}^3/6)$	$[2h\tau_{\rm c}(1-\lambda t_{\rm m})/6]V'''-[(1+2p)/12]V'''$

The following transformations are conducted to derive the standardized equation:

$$T'=g_1T,\quad R=\sqrt{\frac{g_1}{g_2}}R'. \tag{29}$$

Then the standard mKdV equation with correction term $O(\varepsilon)$ can be deduced:

$$\partial_{T'}R'-\partial_X^3R'+\partial_X R'^3+\varepsilon M\left[R'\right]=0, \tag{30}$$

where

$$M\left[R'\right]=\frac{g_3}{g_1}\partial_X^2R'+\frac{g_4}{g_1}\partial_X^4R'+\frac{g_5}{g_2}\partial_X^2R'^3.$$

If the correction term $O(\varepsilon)$ is neglected, then we can derive the mKdV equation with the following kink–antikink solution:

$$R'_0\left(X,T'\right)=\sqrt{c}\tanh\sqrt{\frac{c}{2}}\left(X-cT'\right). \tag{31}$$

Assume that $R'(X,T')=R'_0(X,T')+\varepsilon R'_1(X,T')$. Here, the correction term $O(\varepsilon)$ is taken into consideration. Before determining the propagation velocity value of the kink solution, we need to consider the following solvability condition first:

$$\left(R'_0,M\left[R'_0\right]\right)\equiv\int_{-\infty}^{+\infty}{\rm d}XR'_0M\left[R'_0\right]=0, \tag{32}$$

where $M[R'_0]=M[R']$. Then the propagation velocity can be calculated, which is expressed by the following formula:

$$c=\frac{5g_2g_3}{2g_2g_4-3g_1g_5}. \tag{33}$$

Therefore, the kink–antikink solution of the mKdV equation is given as

$$R(X,T)=\sqrt{\frac{g_1c}{g_2}}\tanh\sqrt{\frac{c}{2}}\left(X-cg_1T\right). \tag{34}$$

The kink–antikink solution of the headway is obtained as follows:

$$\begin{aligned}\Delta x_n=\;&h_{\rm c}+\sqrt{\frac{g_1c}{g_2}\left(\frac{\tau}{\tau_{\rm c}}-1\right)}\tanh\sqrt{\frac{c}{2}\left(\frac{\tau}{\tau_{\rm c}}-1\right)}\\&\times\left[n+\left(h-cg_1\left(\frac{\tau}{\tau_{\rm c}}-1\right)\right)t\right].\end{aligned} \tag{35}$$

We can also obtain the amplitude of the kink–antikink solution

$$A=\sqrt{\frac{g_1c}{g_2}\left(\frac{\tau}{\tau_{\rm c}}-1\right)}. \tag{36}$$

The above kink–antikink solution is used to characterize the coexisting phase of the traffic flow, which includes both the free-running phase and the congested phase. The dashed lines in Figs. 2 and 3 depict the coexisting curve of the traffic flow, which can be expressed by $\Delta x_n=h_{\rm c}\pm A$.

5. Numerical simulation

To further verify the impact of the self-stabilizing effect on the stability of heterogeneous traffic flow, numerical simulation experiments are carried out in this section.

5.1. Simulation setup

For the convenience of simulation, let $t_0=m\Delta t$, and then the discrete form of the model (8) can be obtained as

$$\begin{aligned}\frac{{\rm d}v_n(t)}{{\rm d}t}=\;&\alpha\left[(1+p)V\left(\Delta x_n(t)\right)-pV\left(\Delta x_{n-1}(t)\right)-v_n(t)\right]\\&+\lambda\left[v_n(t)-\frac{1}{m}\sum_{i=1}^{m}v_n(t-i\Delta t)\right],\end{aligned} \tag{37}$$

where $p=\mu$ for autonomous vehicles and $p=0$ for human-driving vehicles [see Eq. (9)].

The numerical simulations in this section are conducted under the periodic boundary condition. The road length is $L=1700$ m and the total number of vehicles is $N=100$. Without loss of generality, the maximum velocity of all vehicles

is $v_{\max} = 14.67$ m/s and the length of all vehicles is set as $l_n = 5$ m. The simulation time step is taken as $\Delta t = 0.1$ s. The simulation duration is 2×10^5 time steps, and the data were picked up at and after the (1.9×10^5)-th time step.

The initial states of the traffic flow are given as follows:

$$v_n(i) = 0, \quad n = 1,2,\ldots,N, \quad i = 0,1,2,\ldots,m, \tag{38}$$

$$\begin{cases} x_1(i) = 0, \quad i = 0,1,2,\ldots,m, \\ x_{n+1}(i) = x_n(i) + L/N, \quad n \neq 50,51, \quad i = 0,1,2,\ldots,m, \\ x_{51}(i) = x_{50}(i) + L/N - \Delta, \\ x_{52}(i) = x_{51}(i) + L/N + \Delta, \quad \Delta = 5 \text{ m}. \end{cases} \tag{39}$$

The velocity and position of the vehicles are calculated by the following rules:

$$\begin{cases} v_n(t+\Delta t) = v_n(t) + \dfrac{\mathrm{d}v_n(t)}{\mathrm{d}t}\Delta t, \\ x_n(t+\Delta t) = x_n(t) + v_n(t)\Delta t + \dfrac{1}{2}\dfrac{\mathrm{d}v_n(t)}{\mathrm{d}t}\Delta t^2. \end{cases} \tag{40}$$

5.2. Simulation for autonomous vehicles

In this part, the effect of the self-stabilizing coefficient λ and historical time length t_0 on the stability of autonomous vehicle flow is investigated. The model parameters are set as the following values:

(i) $\alpha_{\mathrm{A}} = 1.25$, $\mu = 0.1$, $\lambda = 0, 0.2, 0.5, 0.8$, $t_0 = 0.5$;

(ii) $\alpha_{\mathrm{A}} = 1.25$, $\mu = 0.2$, $\lambda = 0.2$, $t_0 = 0.1, 0.5, 1.0, 1.5$.

The simulation results are shown in Figs. 4–7.

Figure 4 shows the headway profiles of autonomous vehicles at $t = 1.9 \times 10^4$ s under different λ values. From Fig. 4, we can see that compared with the model without self-stabilizing effect ($\lambda = 0$), the model with self-stabilizing effect has a smaller headway fluctuation, which indicates that the self-stabilizing effect can enhance the stability of autonomous vehicle flow. In addition, with the increase of the self-stabilizing coefficient λ, the headway fluctuation gradually decreases. When the self-stabilizing coefficient λ increases to a certain value, the headway no longer fluctuates. Figure 5 shows the space–time evolution of density waves in autonomous vehicle flow after $t = 1.9 \times 10^4$ s under different λ values. The amplitude of density waves decreases with a greater λ value. In addition, the density waves propagate backward with time.

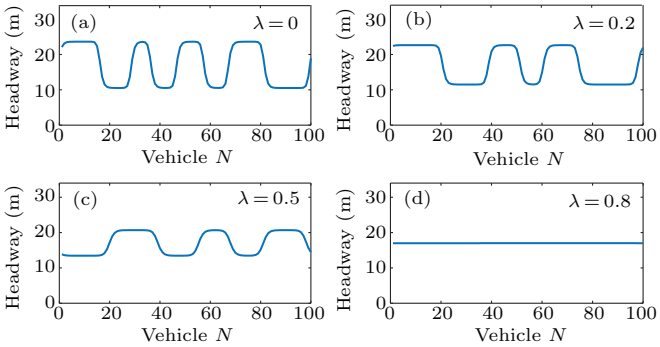


Fig. 4. The headway profiles of autonomous vehicles under different λ values at $t = 1.9 \times 10^4$ s.

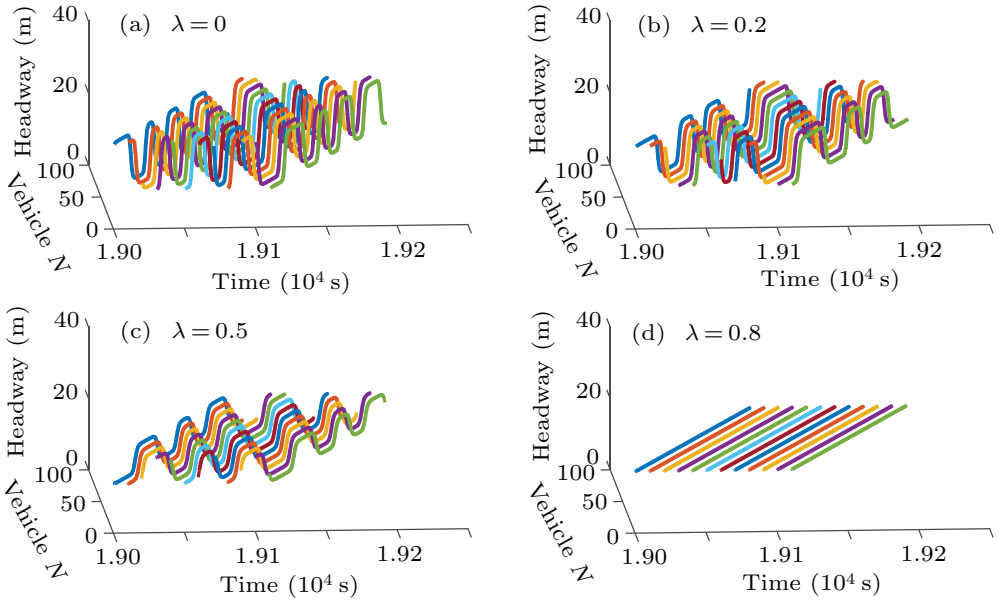


Fig. 5. Space–time evolution of density waves in autonomous vehicles under different λ values after $t = 1.9 \times 10^4$ s.

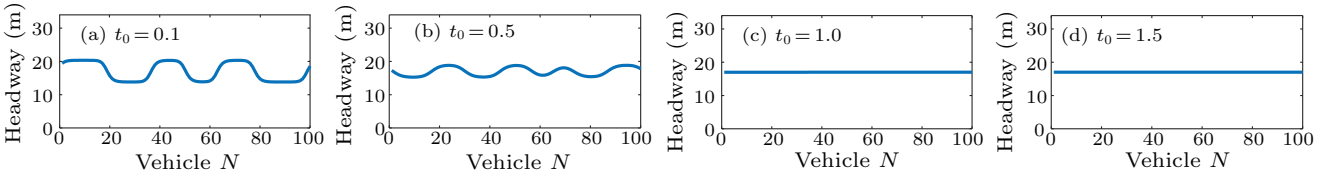


Fig. 6. The headway profiles of autonomous vehicles under different t_0 values at $t = 1.9 \times 10^4$ s.

Figure 6 shows the headway profiles of autonomous vehicles at $t = 1.9 \times 10^4$s under different values of t_0. As the parameter t_0 increases, the variation range of the headway becomes smaller. Figure 7 shows the space–time evolution of density waves in autonomous vehicle flow after $t = 1.9 \times 10^4$ s under different values of t_0. It can be seen from Fig. 7 that increasing the value of t_0 can decrease the amplitude of density waves.

From the above results, we can conclude that the stability of autonomous vehicle flow is strengthened with the increase of the self-stabilizing coefficient or historical time length. This conclusion is consistent with the theoretical results in Section 3.

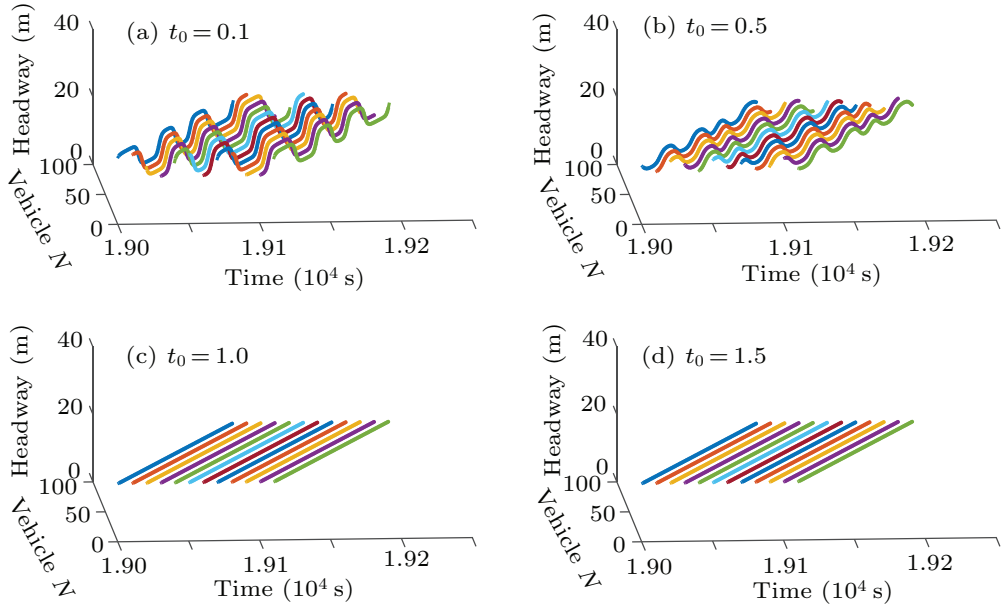


Fig. 7. Space–time evolution of density waves in autonomous vehicles under different t_0 values after $t = 1.9 \times 10^4$ s.

5.3. Simulation for heterogeneous traffic flow

In this part, we conduct numerical simulations in heterogeneous traffic flow. First, the influence of different parameters on the stability of heterogeneous traffic flow is studied. In this experiment, human-driving vehicles and autonomous vehicles are 50% respectively, *i.e.*, the proportion of autonomous vehicles is $\beta = 0.5$. In addition, these two types of vehicles distribute on the road in random order. The sensitivity of human-driving vehicles follows the normal distribution $\alpha_{\mathrm{H}} \sim N\left(0.85, 0.05^2\right)$, and the sensitivity of autonomous vehicles is $\alpha_{\mathrm{A}} = 2.5$. The rest of the parameters are taken as follows:

(i) $\mu = 0.2$, $\lambda = 0$, 0.2, 0.5, 0.8, $t_0 = 0.5$;

(ii) $\mu = 0.2$, $\lambda = 0.2$, $t_0 = 0.1$, 0.5, 1.0, 1.5.

The results are shown in Figs. 8–11.

Figures 8 and 9 show the vehicle trajectories and space–time diagrams of the heterogeneous traffic flow after $t = 1.9 \times 10^4$ s under different λ values, respectively. It can be seen that introducing the self-stabilizing effect in heterogeneous traffic flow can suppress stop-and-go waves and reduce the velocity variation amplitude, so as to enhance the stability of heterogeneous traffic flow. In addition, with the increase of λ, the stop-and-go waves are gradually dissipated and the velocity fluctuation is gradually reduced.

Figures 10 and 11 show the trajectories and space–time diagrams of heterogeneous traffic flow after $t = 1.9 \times 10^4$ s under different t_0 values, respectively. It is shown that a larger t_0 value means a smaller amplitude of stop-and-go waves and a smaller velocity change.

From Figs. 8–11, we can conclude that for heterogeneous traffic flow, increasing the self-stabilizing coefficient or historical time length can also strengthen its stability when the proportion of autonomous vehicles is fixed.

Next, we investigate the relationship between the stability of heterogeneous traffic flow and the proportion of autonomous vehicles β. Model parameters are set as: $\alpha_{\mathrm{H}} \sim N\left(0.85, 0.05^2\right)$, $\alpha_{\mathrm{A}} = 2.5$, $\mu = 0.2$, $\lambda = 0.2$, $t_0 = 0.5$, and the proportion of autonomous vehicles are taken as $\beta = 0$, 0.33, 0.67, 1. The results are shown in Figs. 12 and 13. As the proportion of autonomous vehicles increases, the stop-and-go waves in the heterogeneous traffic flow are gradually suppressed, and the velocity change is gradually decreased. When the proportion of autonomous vehicles increases to a certain value, the stop-and-go waves disappear in the heterogeneous traffic flow, and the velocity of the heterogeneous traffic flow no longer changes. Therefore, increasing the proportion of autonomous vehicles has a positive effect on stabilizing heterogeneous traffic flow and alleviating traffic congestion.

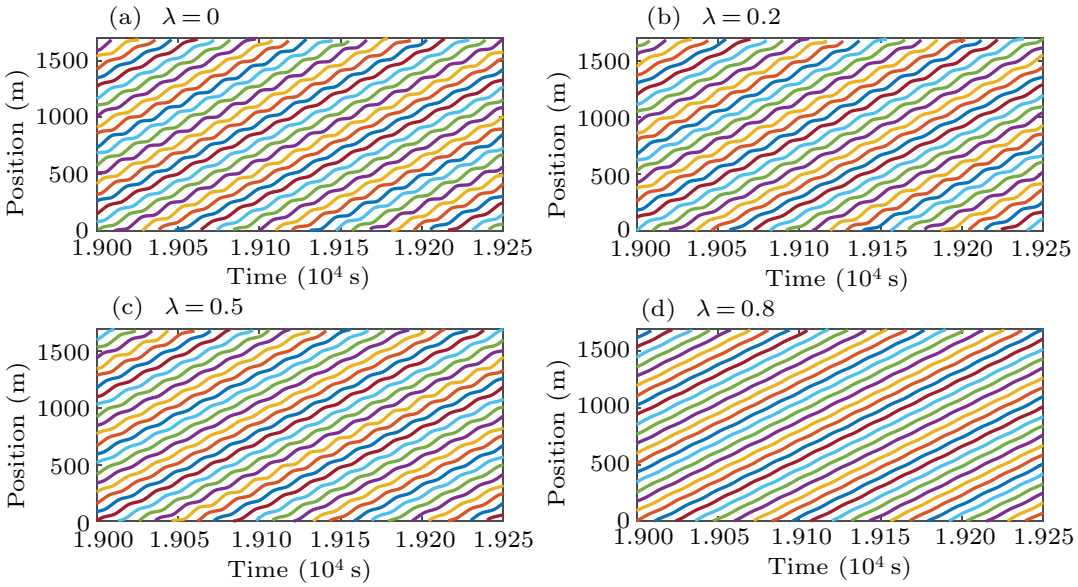


Fig. 8. Vehicle trajectories for every five vehicles in the heterogeneous traffic flow after $t = 1.9 \times 10^4$ s under different λ values ($\beta = 0.5$).

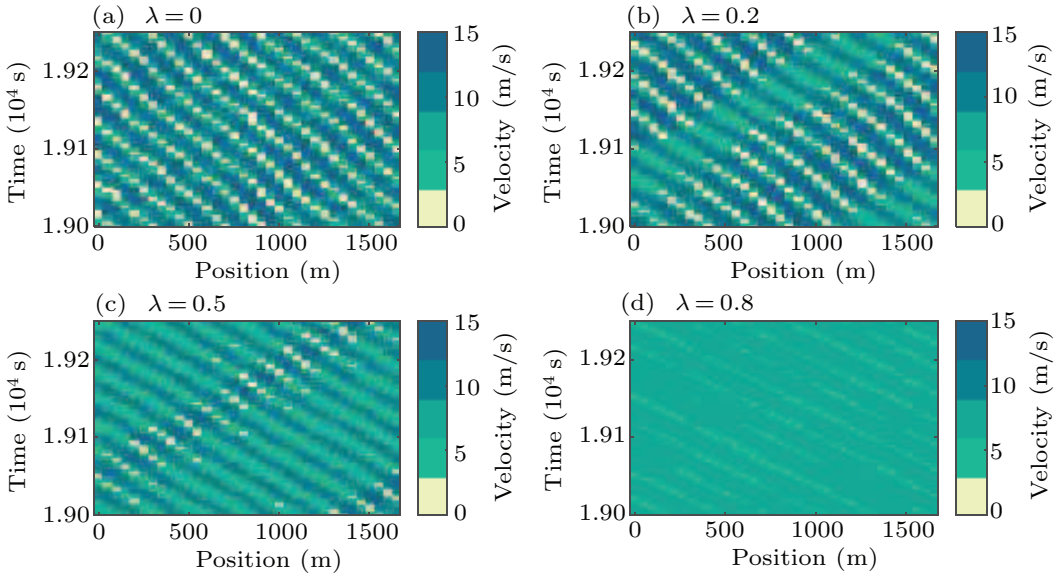


Fig. 9. Space–time diagram of heterogeneous traffic flow after $t = 1.9 \times 10^4$ s under different λ values ($\beta = 0.5$).

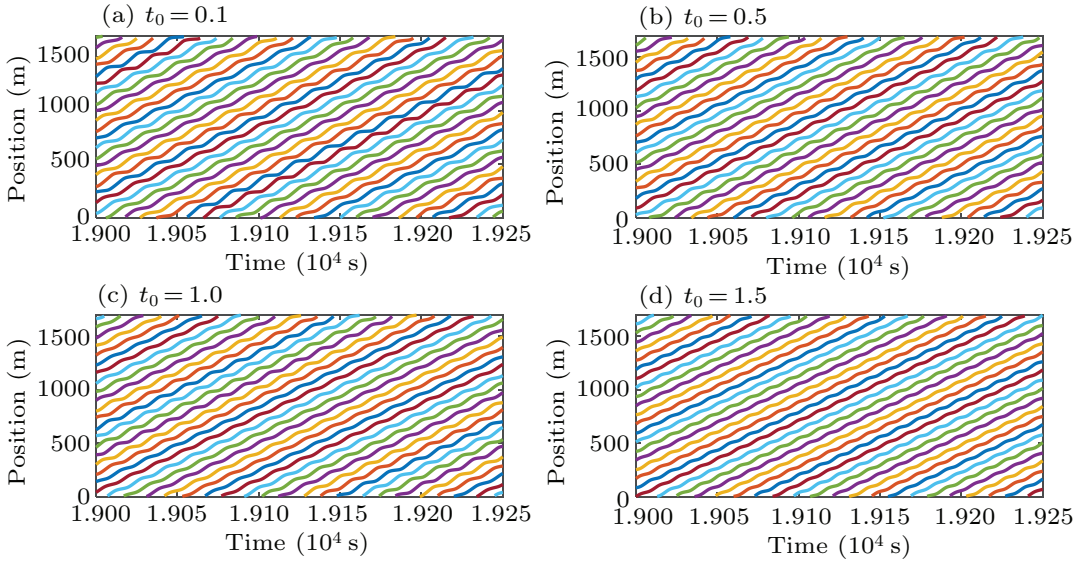


Fig. 10. Vehicle trajectories for every five vehicles in the heterogeneous traffic flow after $t = 1.9 \times 10^4$ s under different t_0 values ($\beta = 0.5$).

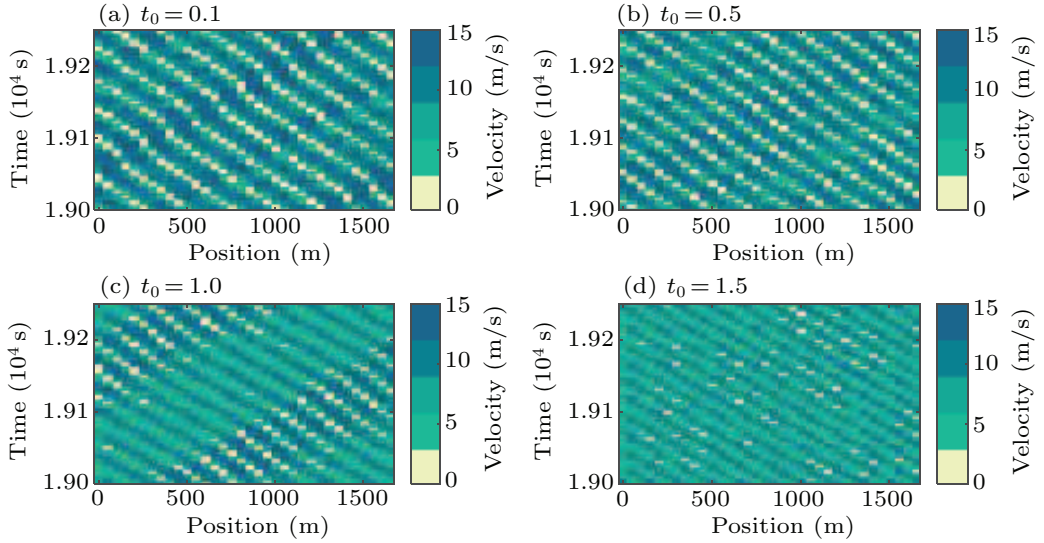


Fig. 11. Space–time diagram of heterogeneous traffic flow after $t = 1.9 \times 10^4$ s under different t_0 values ($\beta = 0.5$).

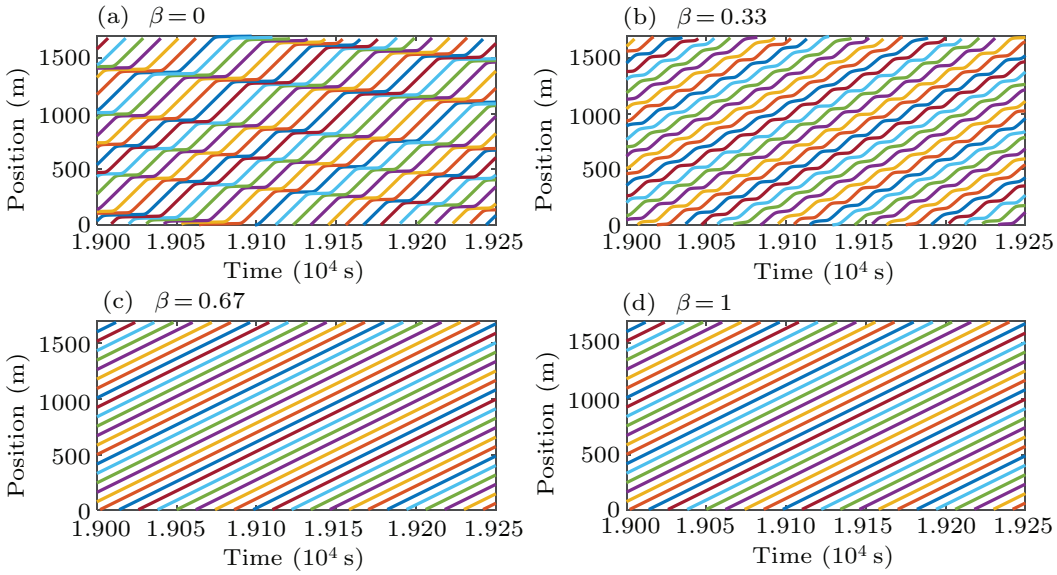


Fig. 12. Vehicle trajectories for every five vehicles in the heterogeneous traffic flow under different proportions of autonomous vehicles β after $t = 1.9 \times 10^4$ s.

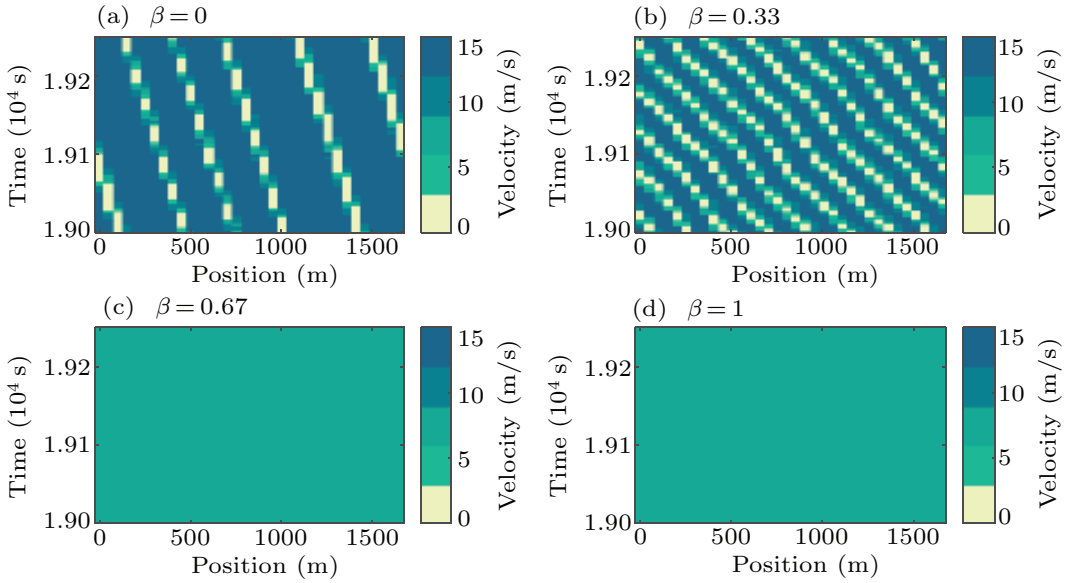


Fig. 13. Space–time diagram of heterogeneous traffic flow under different proportions of autonomous vehicles β after $t = 1.9 \times 10^4$ s.

6. Conclusion and perspectives

In this paper, the heterogeneous traffic flow with human-driving and autonomous vehicles is studied by analytical and numerical methods. First, we propose an extended car-following model for autonomous vehicles and heterogeneous traffic flow. It takes into account the self-stabilizing effect of vehicles, which enables the autonomous vehicle to use the information of both its own and other vehicles to jointly control its driving behavior. Through linear stability analysis, we obtain the linear stability criterion of the proposed model. Then, the mKdV equation of the model is derived by nonlinear analysis, and the corresponding kink–antikink solution is obtained. Finally, numerical simulations are performed to verify the analytical results. The results show that the self-stabilizing effect plays an important role in stabilizing the heterogeneous traffic flow. In addition, whether it is homogeneous traffic flow or heterogeneous traffic flow, increasing the self-stabilizing coefficient or historical time length can strengthen the stability of traffic flow and reduce traffic congestion effectively. This conclusion is in good agreement with the theoretical analysis. Moreover, the stability of the heterogeneous traffic flow can also be enhanced by increasing the proportion of autonomous vehicles.

The model proposed in this paper is a theoretical model, and its results mainly come from the simulation data. The future work is to calibrate the model with the data from real traffic so that the model can describe the real traffic behavior more accurately.

Acknowledgements

Project supported by the National Natural Science Foundation of China (Grant No. 61773243), the Major Technology Innovation Project of Shandong Province, China (Grant No. 2019TSLH0203), and the National Key Research and Development Program of China (Grant No. 2020YFB1600501).

References

[1] Pipes L A 1953 *J. Appl. Phys.* **24** 274
[2] Bando M, Hasebe K, Nakayama A, Shibata A and Sugiyama Y 1995 *Phys. Rev. E* **51** 1035
[3] Nagatani T 1999 *Phys. Rev. E* **60** 6395
[4] Sawada S 2001 *J. Phys. Math. Gen.* **34** 11253
[5] Jiang R, Wu Q and Zhu Z 2001 *Phys. Rev. E* **64** 017101
[6] Ge H X, Zhu H B and Dai S Q 2006 *Eur. Phys. J. B* **54** 503
[7] Li Z P and Liu Y C 2006 *Eur. Phys. J. B* **53** 367
[8] Peng G H, Cai X H, Liu C Q, Cao B F and Tuo M X 2011 *Phys. Lett. A* **375** 3973
[9] Liu Y J, Zhang H L and He L 2012 *Chin. Phys. Lett.* **29** 104502
[10] Yu S, Liu Q and Li X 2013 *Commun. Nonlinear Sci. Numer. Simul.* **18** 1229
[11] Tang T, Shi W, Shang H and Wang Y 2014 *Nonlinear Dyn.* **76** 2017
[12] Tang T Q, Li J G, Huang H J and Yang X B 2014 *Measurement* **48** 63
[13] Li Z, Li W, Xu S and Qian Y 2015 *Nonlinear Dyn.* **80** 529
[14] Li Z, Qin Q, Li W, Xu S, Qian Y and Sun J 2018 *Nonlinear Dyn.* **91** 1113
[15] Peng G, Lu W, He H and Gu Z 2016 *Commun. Nonlinear Sci. Numer. Simul.* **40** 197
[16] Liu F, Cheng R, Ge H and Yu C 2016 *Physica A* **464** 267
[17] Ou H, Tang T Q, Zhang J and Zhou J M 2018 *Physica A* **505** 105
[18] Zhang J, Tang T Q and Yu S W 2018 *Physica A* **492** 1831
[19] Chen C, Ge H and Cheng R 2019 *Physica A* **535** 122423
[20] Sun Y, Ge H and Cheng R 2019 *Physica A* **521** 752
[21] Liao P, Tang T Q, Wang T and Zhang J 2019 *Physica A* **525** 108
[22] Kuang H, Wang M T, Lu F H, Bai K Z and Li X L 2019 *Physica A* **527** 121268
[23] An S, Xu L, Chen G and Shi Z 2020 *Mod. Phys. Lett. B* **34** 2050182
[24] Li S, Cheng R and Ge H 2020 *Physica A* **558** 125015
[25] Peng G H 2020 *Chin. Phys. B* **29** 084501
[26] Peng Y, Liu S and Yu D Z 2020 *Physica A* **538** 122967
[27] Ma M, Ma G and Liang S 2021 *Appl. Math. Model.* **94** 1
[28] Cheng R, Li S and Ge H 2021 *Mod. Phys. Lett. B* **35** 2150238
[29] Kuang H, Lu F H, Yang F L, Peng G H and Li X L 2021 *Int. J. Mod. Phys. C* **32** 2150095
[30] Zhou Y and Ahn S 2019 *Transp. Res. Part B* **125** 175
[31] Xu S and Peng H 2020 *IEEE Trans. Intell. Transp. Syst.* **21** 48
[32] Xu C, Zhao W and Wang C 2020 *IEEE Trans. Intell. Transp. Syst.* **21** 2510
[33] Xia Y, Qu Z, Sun Z and Li Z 2021 *IEEE Trans. Veh. Technol.* **70** 4178
[34] Tang T Q, Gui Y and Zhang J 2021 *IEEE Trans. Intell. Transp. Syst.*
[35] Bose A and Ioannou P A 2003 *IEEE Trans. Intell. Transp. Syst.* **4** 173
[36] Ngoduy D 2013 *Commun. Nonlinear Sci. Numer. Simul.* **18** 2699
[37] Zhu W X and Zhang H M 2018 *Physica A* **496** 274
[38] Gong S and Du L 2018 *Transp. Res. Part B* **116** 25
[39] Navas F and Milanés V 2019 *Transp. Res. Part C* **108** 167
[40] Xie D F, Zhao X M and He Z 2019 *IEEE Trans. Intell. Transp. Syst.* **20** 2060
[41] Di Vaio M, Fiengo G, Petrillo A, Salvi A, Santini S and Tufo M 2019 *IEEE Trans. Intell. Transp. Syst.* **20** 4339
[42] An S, Xu L, Qian L, Chen G, Luo H and Li F 2020 *Physica A* **560** 125246
[43] Wang J, Zheng Y, Xu Q, Wang J and Li K 2021 *IEEE Trans. Intell. Transp. Syst.* **22** 7445
[44] Zheng F, Liu C, Liu X, Jabari S E and Lu L 2020 *Transp. Res. Part C* **112** 203
[45] Wang S, Yu B and Wu M 2021 *IEEE Trans. Intell. Transp. Syst.*
[46] Montanino M and Punzo V 2021 *Transp. Res. Part B* **144** 133
[47] Yao Z, Xu T, Jiang Y and Hu R 2021 *Physica A* **561** 125218
[48] Guo J, Cheng S and Liu Y 2021 *IEEE Trans. Intell. Transp. Syst.* **22** 1639
[49] Cui S, Cao F, Yu B and Yao B 2021 *IEEE Trans. Intell. Transp. Syst.*
[50] Chen C, Xu Z and Kuang H 2017 *J. Guangxi Normal University* (Natural Science Edition) **35** 14 (in Chinese)
[51] Zhu W X and Zhang L D 2014 *Int. J. Mod. Phys. C* **25** 1450018